6302

NRL Report 6293
AFML-TR-64-408

UNCLASSIFIED

Electron Microscope Fracture Examination to Characterize and Identify Modes of Fracture

C. D. BEACHEM

Physical Metallurgy Branch
Metallurgy Division

September 28, 1965

U.S. NAVAL RESEARCH LABORATORY
Washington, D.C.

CONTENTS

ELECTRON MICROSCOPE FRACTURE EXAMINATION TO CHARACTERIZE AND IDENTIFY MODES OF FRACTURE

1. INTRODUCTION

The examination and study, in the electron microscope, of replicas of fracture surfaces has proved very useful in studies of fracture mechanisms. Fine-scale fracture surface features that are characteristic of specific causes of fracture in specific materials have been recognized in the past as a sufficient basis for the performance of certain failure analyses and of invaluable aid in performing others. However, research into fracture mechanisms and the systematic collection of electron fractographs from well documented fractures are primary necessities for the performance of failure analyses through the use of electron fractography.

The specific aims in this program were: (1) to continue the NRL collection of electron fractographs which characterize fracture surfaces created in the laboratory under known conditions, (2) to investigate fracture mechanisms basic to certain types of fracture, (3) to use electron fractography in the performance of critical failure analyses, (4) to provide guidance to Douglas Aircraft Company during the compilation of the Failure Analysis Handbook, and (5) to train personnel in the techniques of replication and interpretation of electron fractographs.

Specimens with documented histories were obtained from various sources within the Metallurgy and Mechanics Divisions of NRL after they had been fractured in the routine execution of various fracture toughness evaluation programs. None of the specimens were broken specifically for the present contract. Since each NRL Group that supplied specimens for this program was collecting only the data they felt were significant, some of the results reported herein are not complete in all respects. For example, some of the fatigue surfaces examined were fatigue-cracked in order to provide a sharp notch for crack toughness evaluations, and no records of the fatigue stresses were kept.

The cellulose acetate replication process was used almost exclusively in the preparation of replicas. The standard practice was to use 5 mil tape, shadow with palladium at 45° (in the direction of macroscopic crack propagation) and rotate the plastic replica while carbon was evaporated at about 45° angle. The carbon replicas were then freed from the cellulose acetate by washing the replicas in three baths of acetone. In a few instances direct carbon replicas were used. Technique details in these instances are described along with the discussion of the fracture surfaces.

Shadowing direction is indicated in each fractograph by an arrow above the micron marker.

In sampling the fracture surfaces, replicas were made of five or six locations on large specimens. Only the square, or plane strain, fracture surfaces were examined in most instances. Each carbon-backed replica was then cut into grid-size pieces and each piece was studied in the microscope. In each case an overly sufficient number of fractographs were made to make certain of a good characterization. Only those pictures necessary for describing the characteristic features are included in this report.

2. CHARACTERIZATION OF ALUMINUM ALLOY FRACTURE SURFACES

a. 2020 T651

Figures 1-12 are taken from two 2020 T651 aluminum plate specimens fatigue-cracked and broken in an Izod machine which had been modified to hold full-thickness

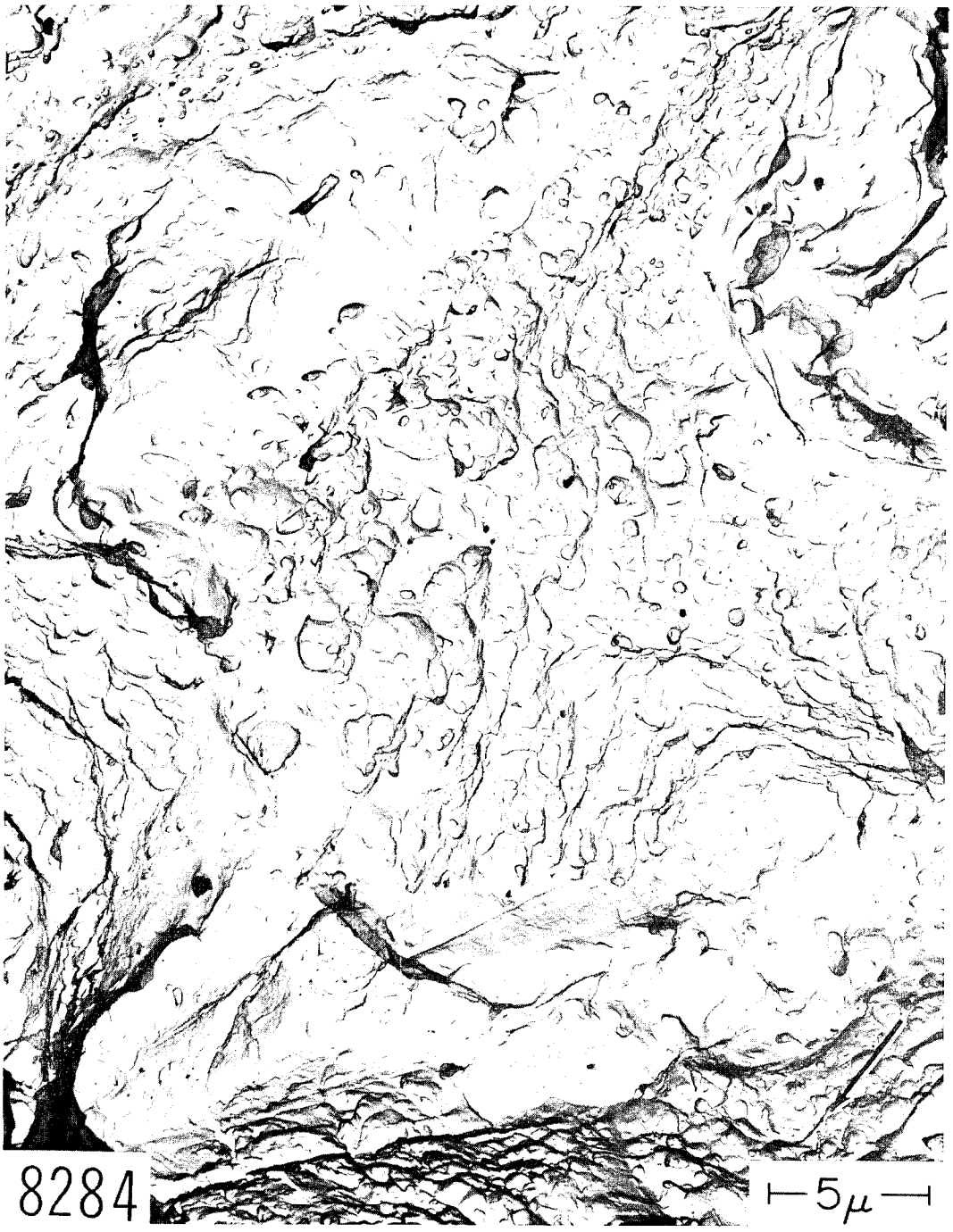

Fig. 1 - Room temperature impact square fracture plane-strain dimpled rupture in 2020 T651 aluminum alloy. Scraping artifacts are evident at the bottom of the fractograph. Cellulose acetate-carbon replication technique. Palladium shadowed. 6000X

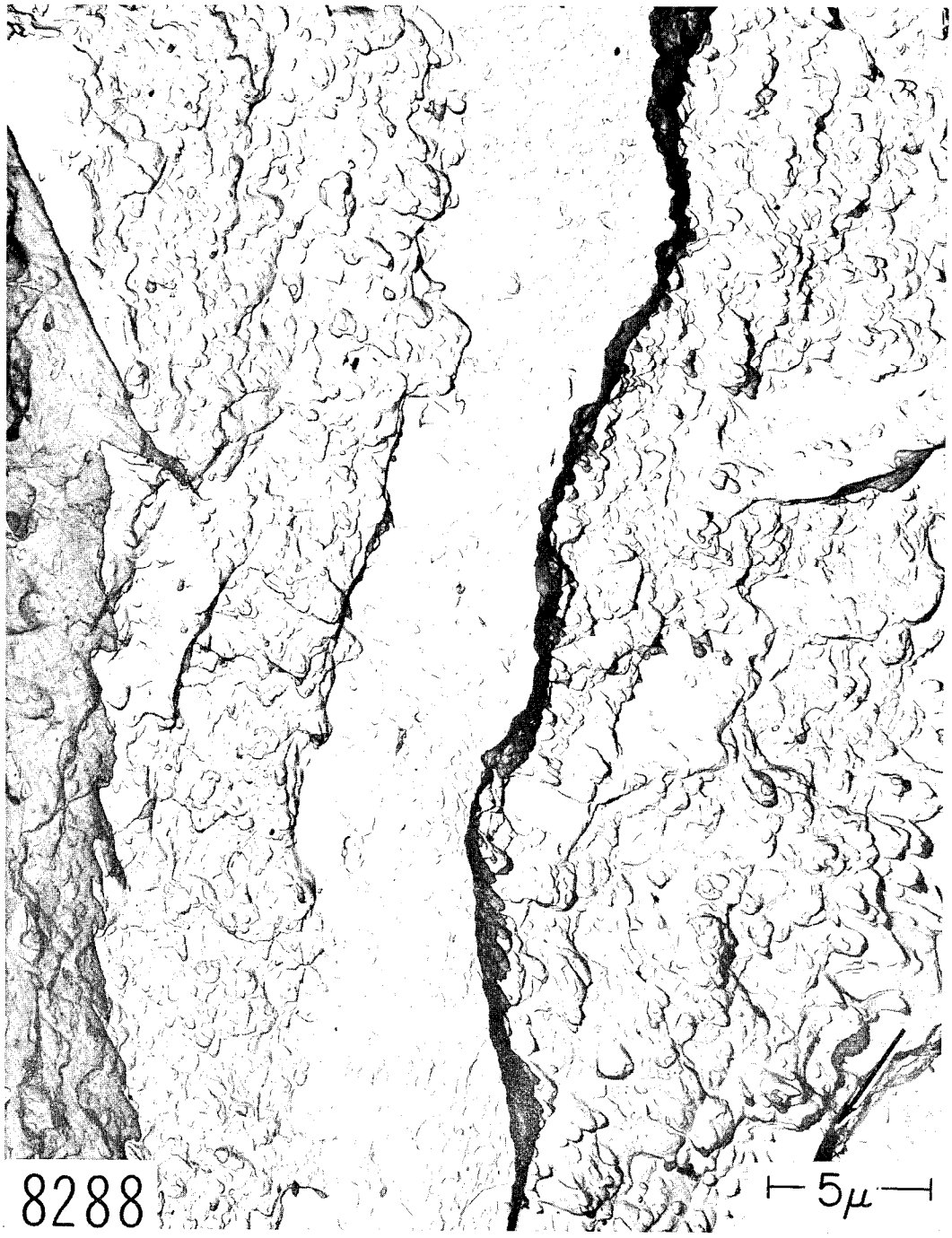

Fig. 2 - Room temperature impact square fracture plane-strain dimpled rupture in 2020 T651 aluminum alloy. Cellulose acetate-carbon replication technique. Palladium shadowed. 6000X.

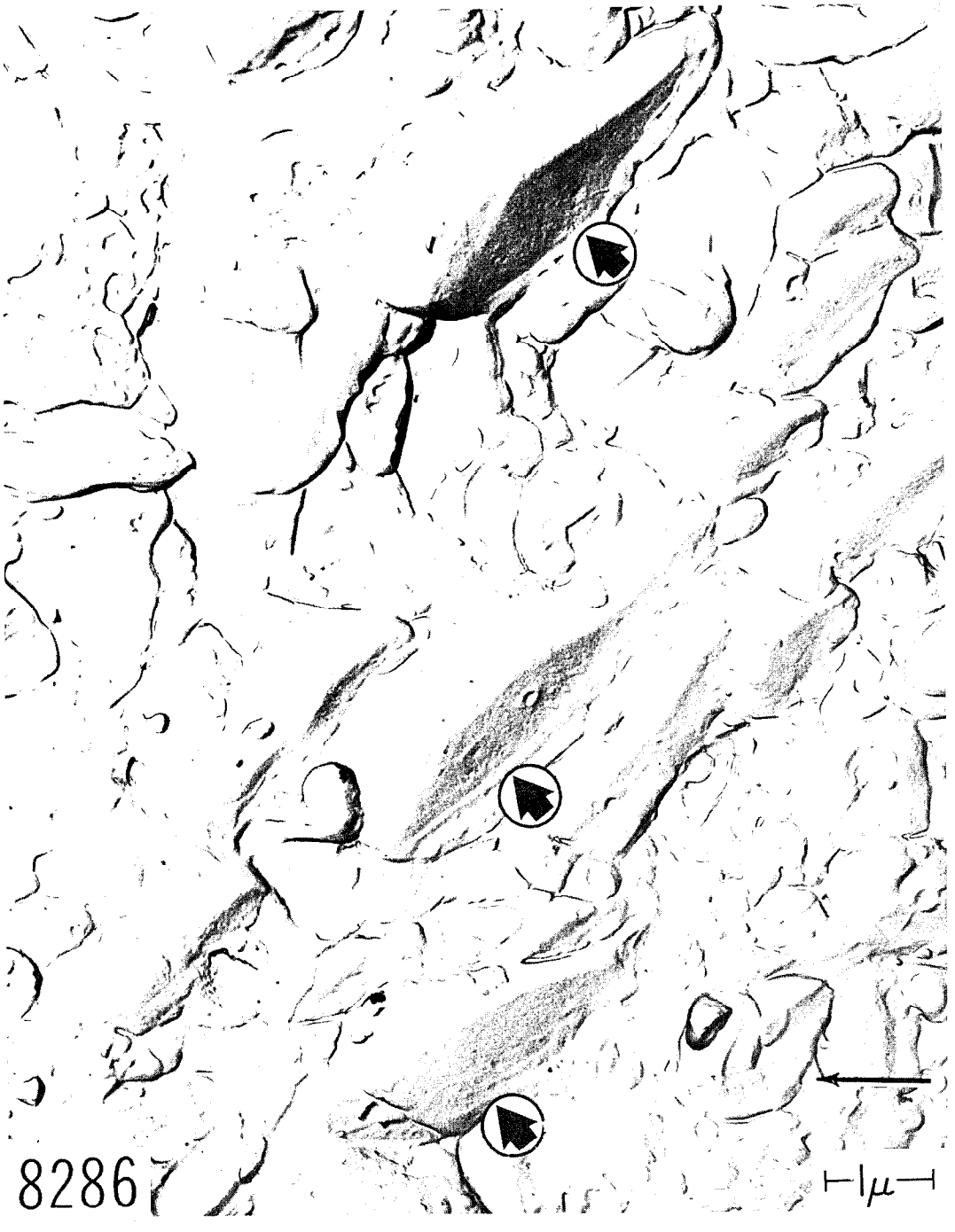

Fig. 3 - Room temperature impact square fracture plane-strain dimpled rupture in 2020 T651 aluminum alloy. Arrows indicate flat plate-like particles often associated with dimples in this material. Cellulose acetate-carbon replication technique. Palladium shadowed. 21,000X.

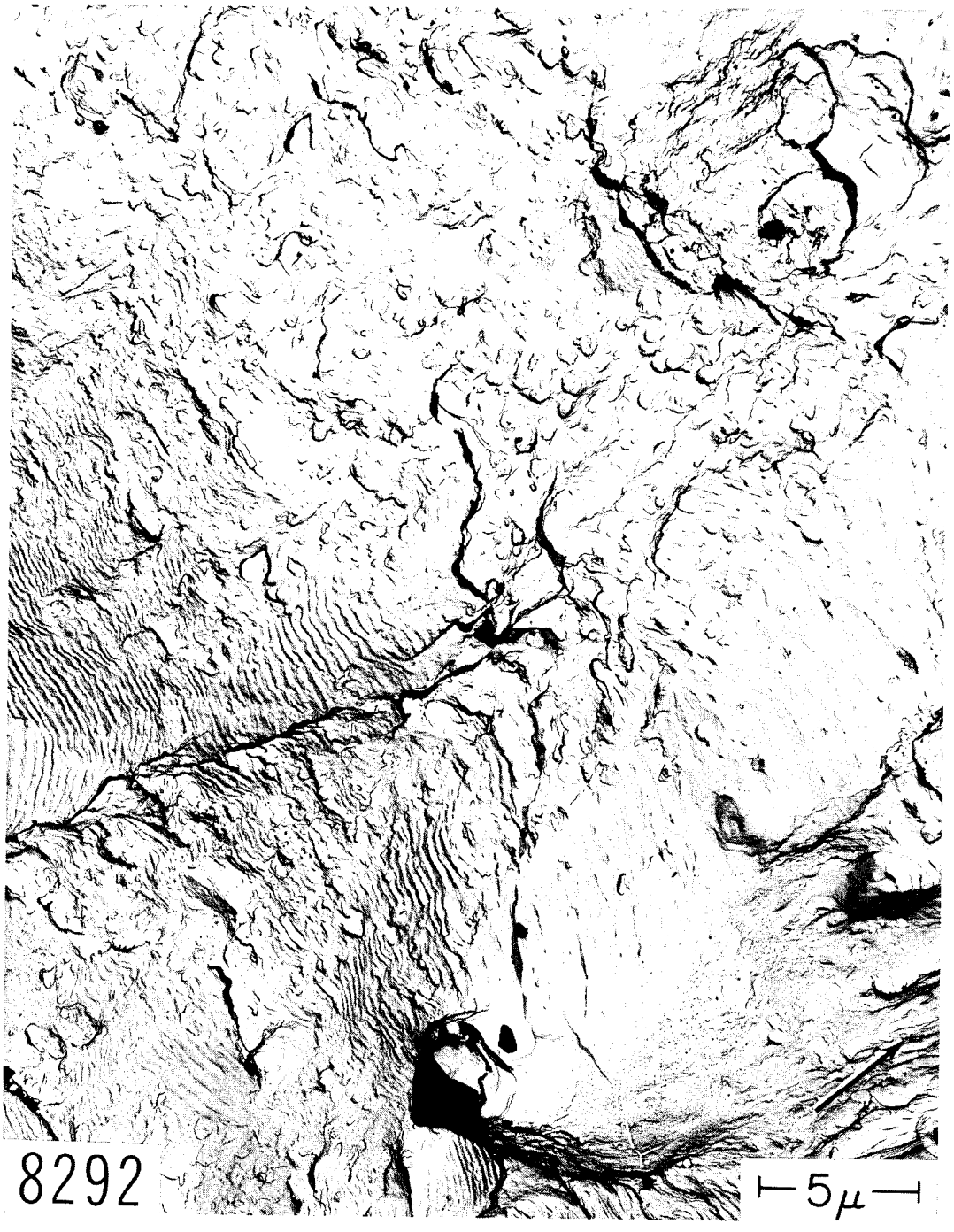

Fig. 4 - Tension-tension plane-strain fatigue markings in an RW fatigue crack in 2020 T651 aluminum alloy. Striations are often mixed with tear dimples. Cellulose acetate-carbon replication technique. Palladium shadowed. 6000X.

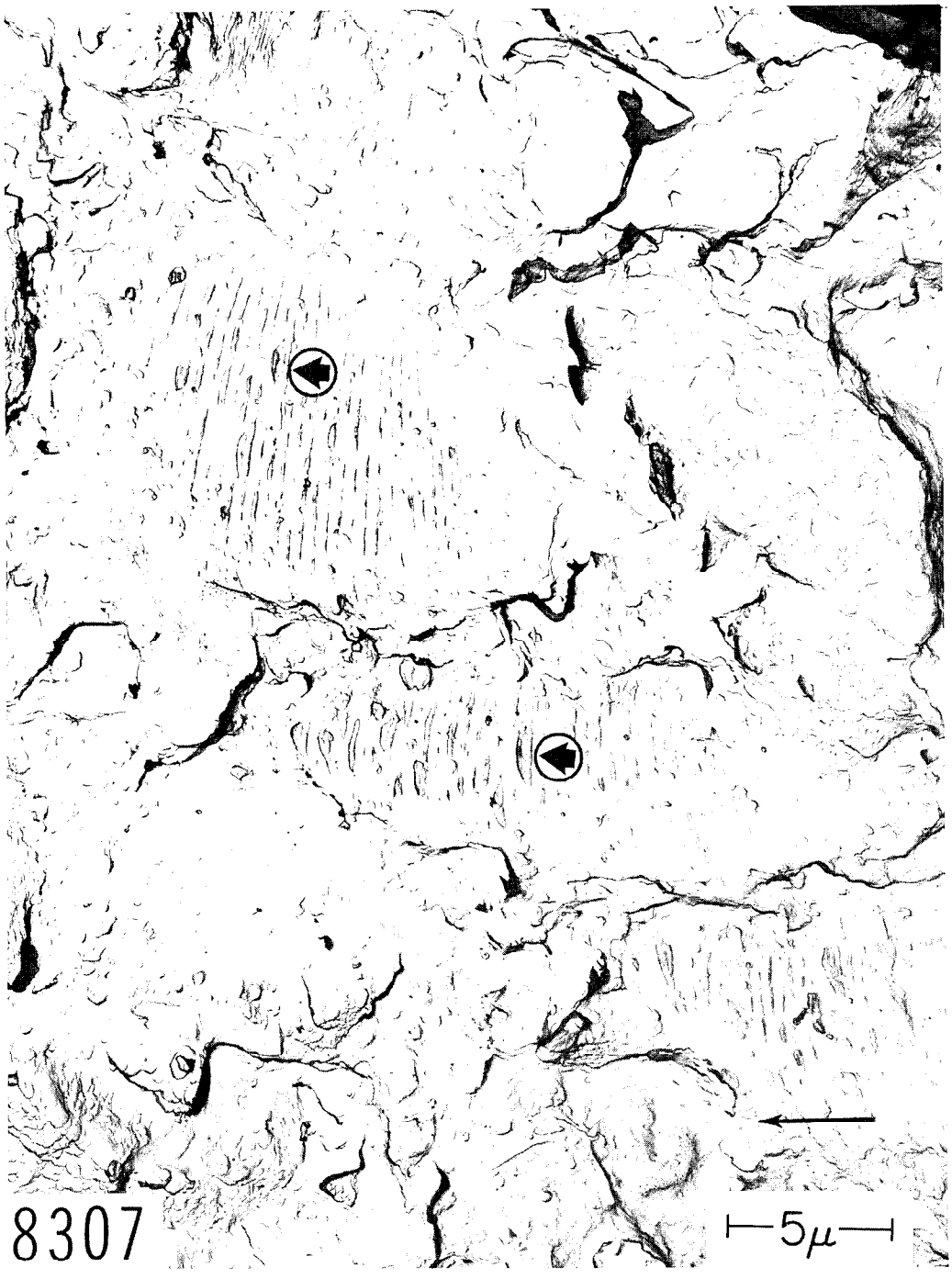

Fig. 5 - Tension-tension plane-strain fatigue markings in an RW fatigue crack in 2020 T651 aluminum alloy. Arrows indicate tongue-shaped cracks along parts of some of the striations. Cellulose acetate-carbon replication technique. Palladium shadowed. 6000X.

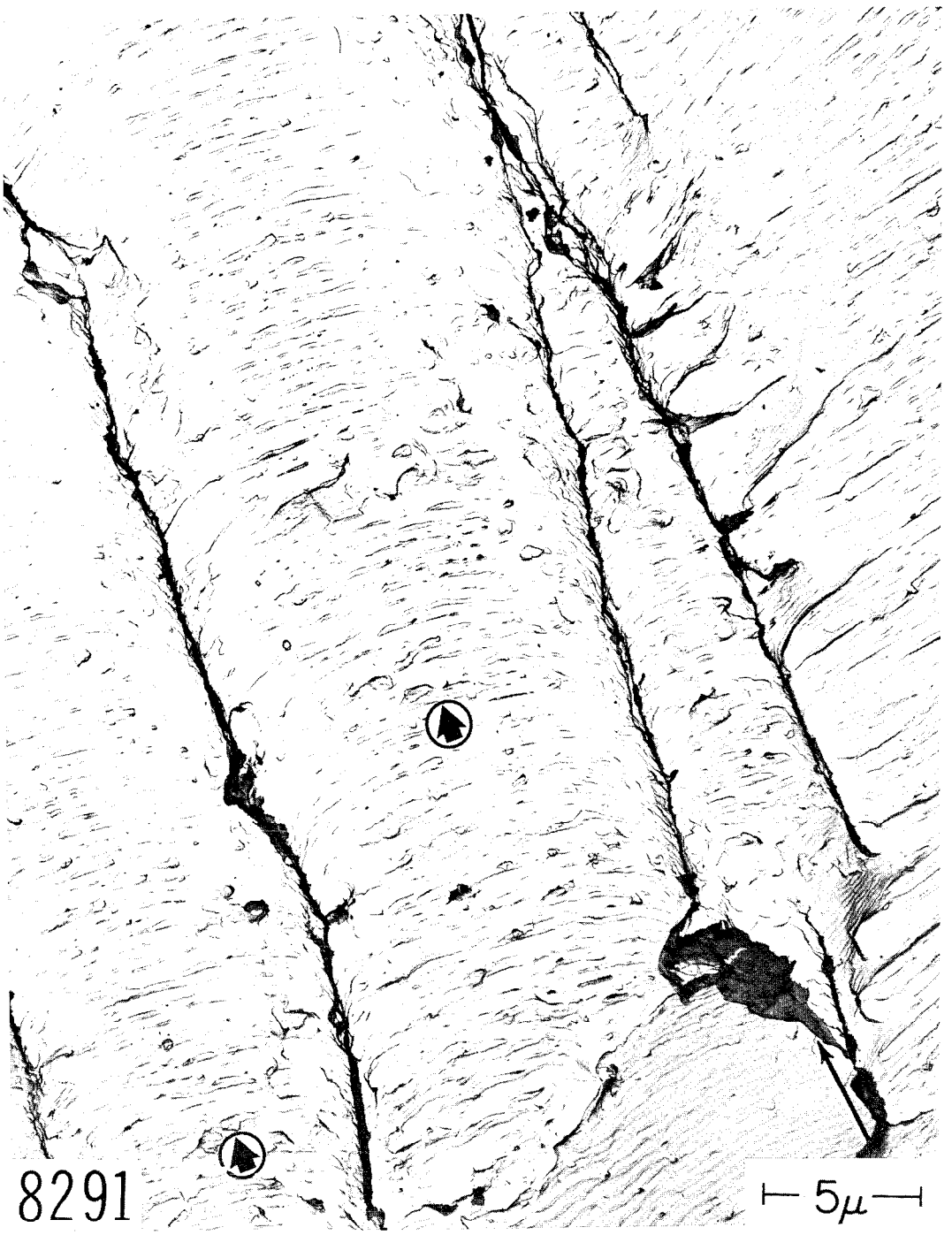

Fig. 6 - Tension-tension plane-strain fatigue markings in an RW fatigue crack in 2020 T651 aluminum alloy. Arrows indicate tongue-shaped cracks along parts of some of the striations. Cellulose acetate-carbon replication technique. Palladium shadowed. 6000X.

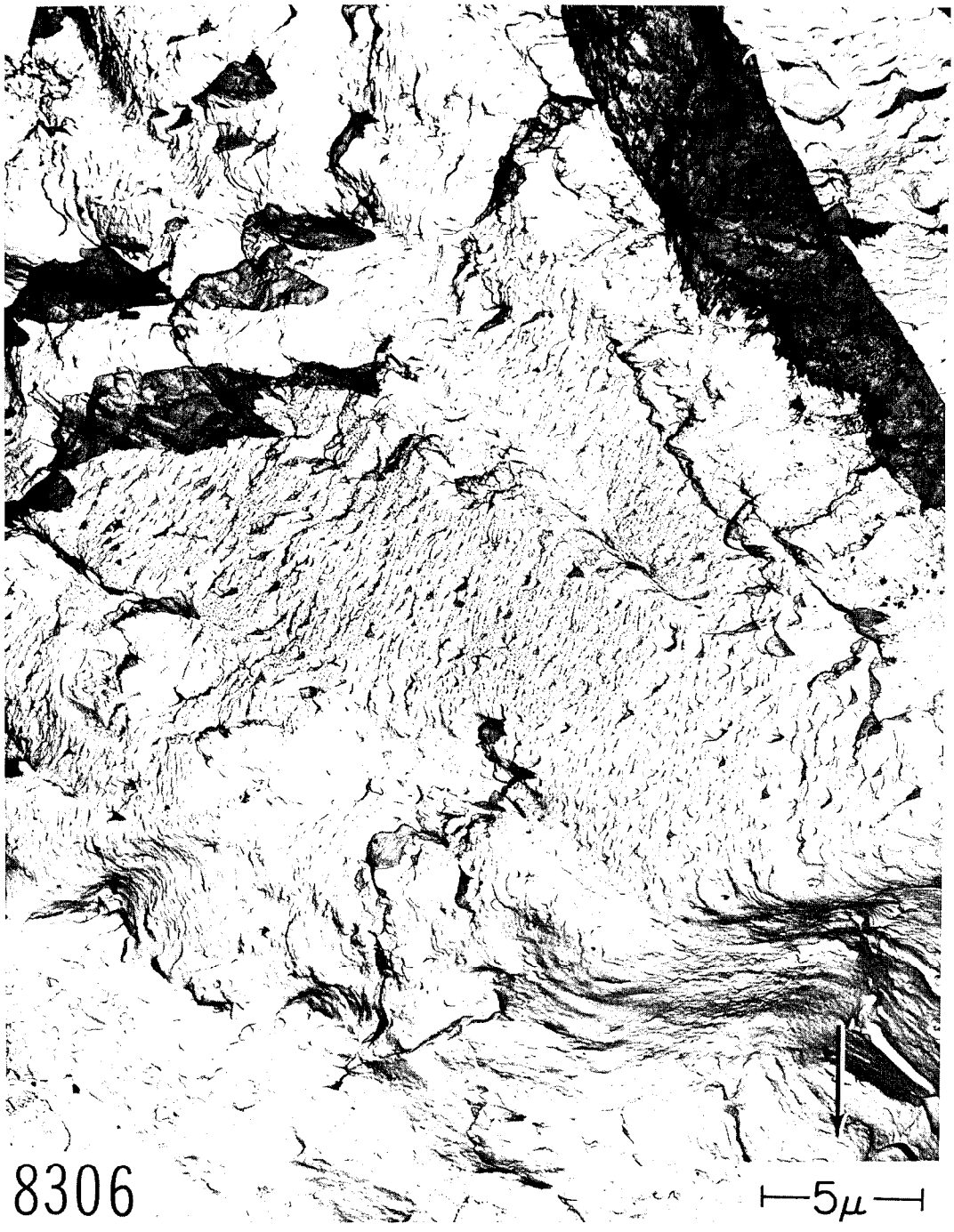

Fig. 7 - Tension-tension plane-strain fatigue markings in the WR fracture direction in 2020 T651 aluminum alloy. Cellulose acetate-carbon replication technique. Palladium shadowed. 6000X.

Fig. 8 - Tension-tension plane-strain fatigue markings in the WR fracture direction in 2020 T651 aluminum alloy. Cellulose acetate-carbon replication technique. Palladium shadowed. 6000X.

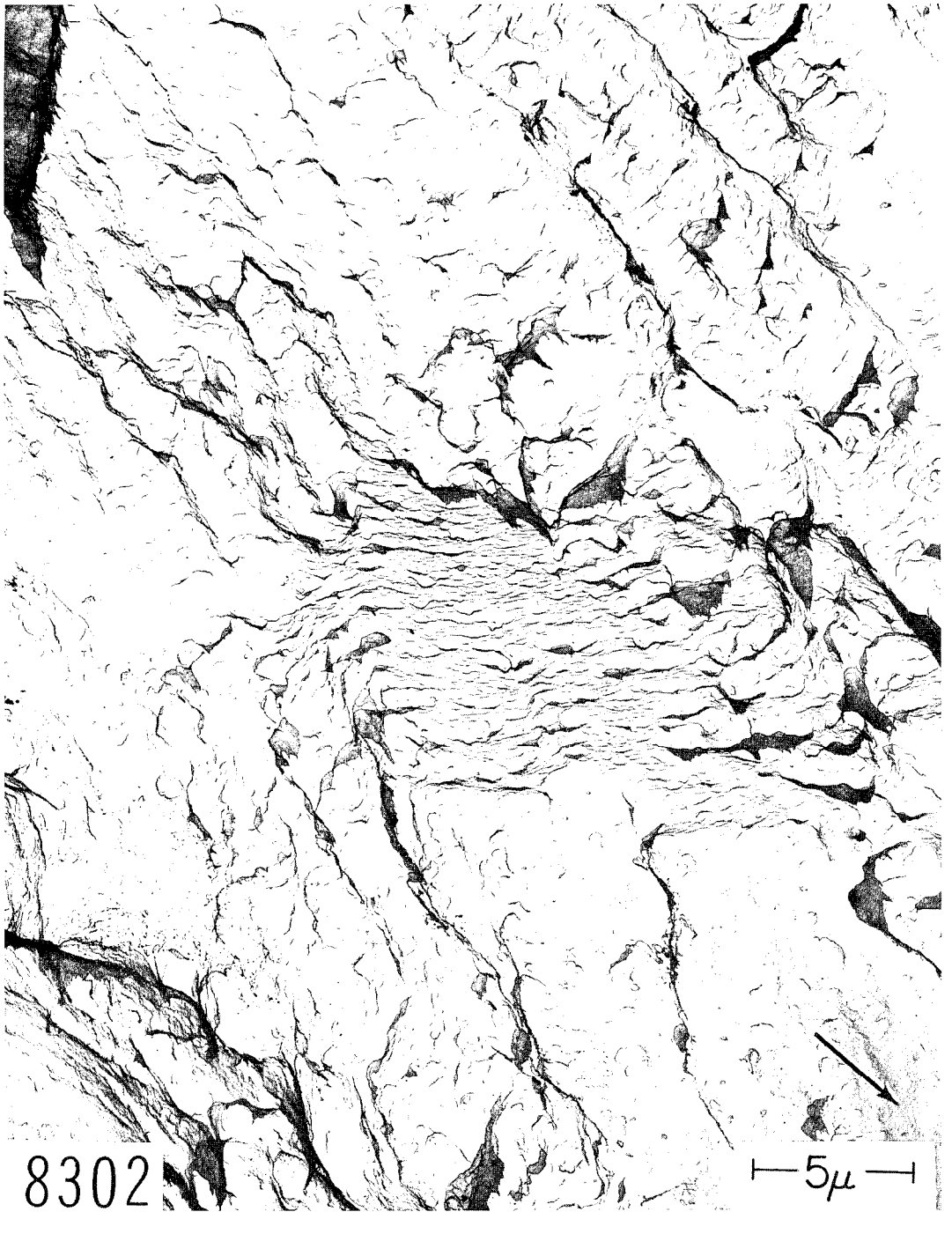

Fig. 9 - Tension-tension plane-strain fatigue markings in the WR fracture direction in 2020 T651 aluminum alloy. Cellulose acetate-carbon replication technique. Palladium shadowed. 6000X.

Fig. 10 - Tension-tension plane-strain fatigue markings in the WR fracture direction in 2020 T651 aluminum alloy. Cellulose acetate-carbon replication technique. Palladium shadowed. 6000X.

Fig. 11 - Tension-tension plane-strain fatigue markings in the WR fracture direction in 2020 T651 aluminum alloy. Cellulose acetate-carbon replication technique. Palladium shadowed. 6000X.

Fig. 12 - Tension-tension plane-strain fatigue markings in the WR fracture direction in 2020 T651 aluminum alloy. Short deep cracks are indicated by arrows. Cellulose acetate-carbon replication technique. Palladium shadowed. 6000X.

plate specimens. The specimens were 3/4 in. thick, 2 in. wide, and 5 in. long. The fatigue cracks were propagated under tension-tension loading (2000 pounds to 5000 pounds) at 3600 cycles per minute. The specimens were broken after precracking by impact loading. One specimen was tested in the TW direction.* The impact energies for both specimens were about 15 foot pounds. Plane strain fracture surfaces are shown in Figs. 1-3. Though these were taken from the RW specimen, they are characteristic of the fracture surface features of the plane strain surfaces in both specimens. Figure 1 shows typical dimples and some scraping artifacts (2). Figure 2 shows what is probably the effect of a banded structure. Figure 3 shows some of the flat regions (arrows) that were often associated with dimples. The fatigue markings for the RW direction are shown in Figs. 4-6. Figures 4 and 5 show that the fatigue markings often were mixed with tear dimples. Figures 5 and 6 show that striations often had tongue-shaped cracks (arrows) along parts of their lengths. Figures 7-12 show the fatigue markings found on the WR fracture surface. In Figs. 7 and 8, the fatigue markings are largely of the usual type (expected in aluminum alloys). However, Figs. 9-12 show, in increasing order, some markings that are not nicely shaped, smoothly curved groups of striations, but consist of short deep cracks as evidenced by thin films of carbon standing in relief on the replica surface (arrows in Fig. 12). Figure 12 also shows a patch of dimples in the upper portion.

b. 2024 T851 and T4

Specimens from three orientations (RW, WR, TR) were cut from a 5-in. thick plate of 2024 T851. The specimens were prepared and tested in the Mechanics Division and were of the short Single Edge Notched (SEN) type - 1/4 in. × 1-1/2 in. × 3.3 in. The fracture toughness values were 46.2 KSI $\sqrt{\text{in.}}$ for the RW direction, 37.5 KSI $\sqrt{\text{in.}}$ for the WR direction, and 23.2 KSI $\sqrt{\text{in.}}$ for the TR direction. The fatigue precracks were made in bending on a lathe and no records of the stresses were made. Figures 13-24 show the influence of orientation on the appearance of the fatigue markings. Figures 13-16 show the RW markings to be, in general, evenly spaced, gently curved striations arranged in groups that are separated by steps (black near-vertical lines in Fig. 15).

Figures 17-20 show typical fatigue surface features in the WR direction. The first three fractographs show short, deep cracks (arrows in Fig. 17) while the fourth (Fig. 20) shows a rather smooth surface. Figure 18 shows a "river pattern" of steps with the same sense of convergence that is found in cleavage (i.e., the fracture propagates down-river). It is also apparent in Fig. 18 that individual segments of the local fatigue crack propagated on different planes. The near horizontal dark bands across the top (between the large arrows) are examples of fatigue on a set of planes whose orientation as a group is different from that of the region as a whole. This strongly suggests a crystallographic influence on the fatigue mechanisms, with the fatigue crack segments possibly seeking to propagate along certain crystallographic planes. A number of these segments (small arrows) are seen to be replicated partially as secondary cracks and partially as portions of the major fracture surface.

Figures 21-24 show typical markings on the fracture surface created by propagating a fatigue crack in the TR direction. Figures 21 and 22 show large numbers of short secondary cracks that are approximately parallel to one another (their lengths extend in a direction from upper left to lower right). Figures 23 and 24 show markings that are much less systematic in their shapes, sizes, and orientations.

A 2024 T4 specimen of the Lehigh bend fatigue type (3), in which a surface crack was caused to propagate by high strain, balanced-cycle, tension-compression loading, yielded the fatigue markings shown in Figs. 25 and 26. This fatigue crack was propagated in the RW direction with the resulting fracture surface features having the same general characteristics as those shown for the same orientation in the previous specimens (Figs. 13-16).

*The ASTM designations of fracture directions are used in this report (1).

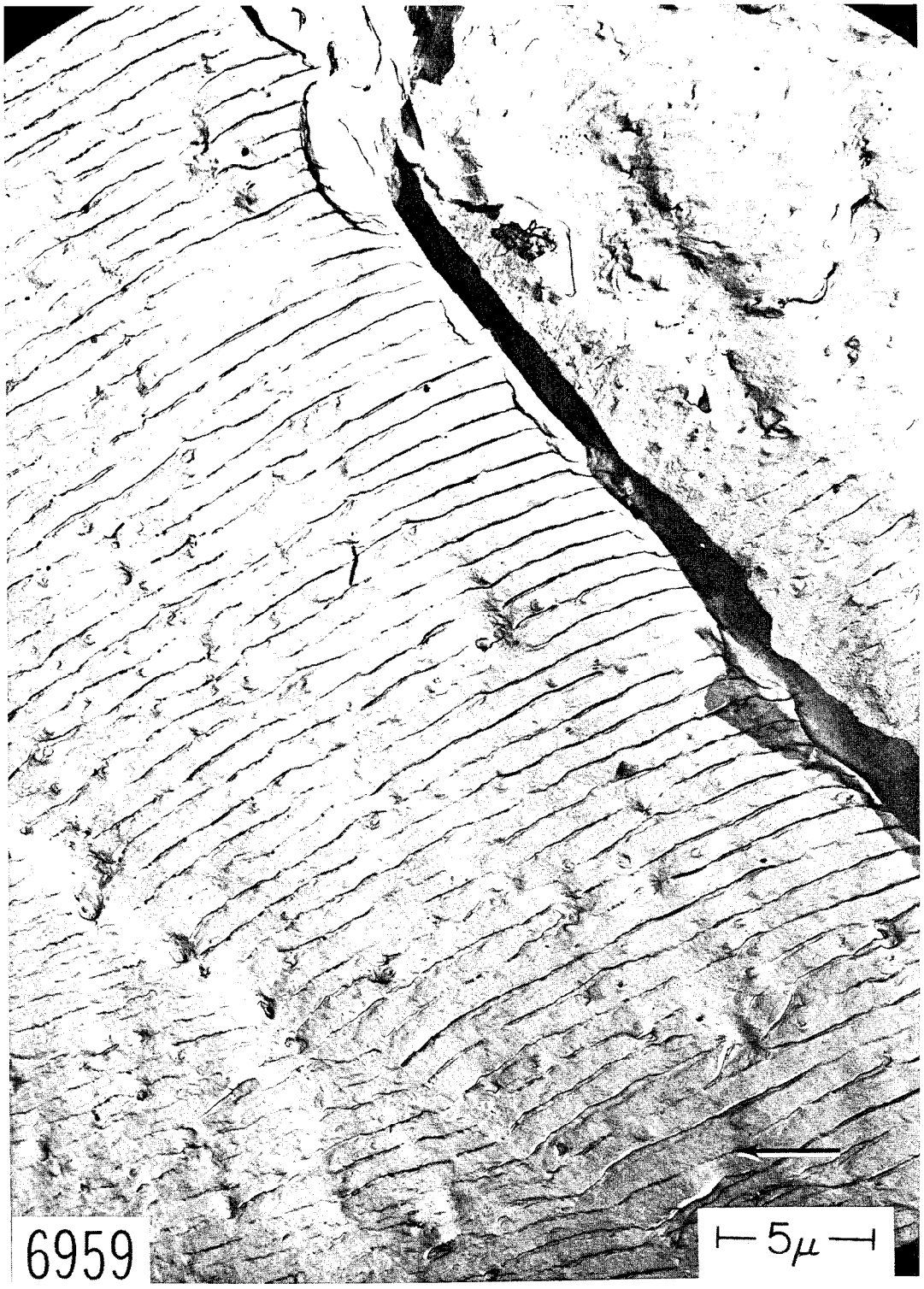

Fig. 13 - Tension-tension plane-strain RW fatigue markings in 2024 T851 aluminum alloy plate. Cellulose acetate-carbon replication technique. Palladium shadowed. 6000X.

Fig. 14 - Tension-tension plane-strain RW fatigue markings in 2024 T851 aluminum alloy plate. Cellulose acetate-carbon replication technique. Palladium shadowed. 6000X.

Fig. 15 - Tension-tension plane-strain RW fatigue markings in 2024 T851 aluminum alloy plate. Cellulose acetate-carbon replication technique. Palladium shadowed. 6000X.

Fig. 16 - Tension-tension plane-strain RW fatigue markings in 2024 T851 aluminum alloy plate. Cellulose acetate-carbon replication technique. Palladium shadowed. 6000X.

Fig. 17 - Tension-tension plane-strain WR fatigue markings in 2024 T851 aluminum alloy plate. Cellulose acetate-carbon replication technique. Palladium shadowed. 6000X.

Fig. 18 - Tension-tension plane-strain WR fatigue markings in 2024 T851 aluminum alloy plate. Cellulose acetate-carbon replication technique. Palladium shadowed. 6000X.